PERGAMON

Journal of Structural Geology 25 (2003) 455–467

JOURNAL OF STRUCTURAL GEOLOGY

www.elsevier.com/locate/jsg

Geophysical exploration within northern Devils Lane graben, Canyonlands National Park, Utah: implications for sediment thickness and tectonic evolution

E.B. Grosfils[a,*], R.A. Schultz[b], G. Kroeger[c]

[a]*Geology Department, Pomona College, 609 N. College Avenue, Claremont, CA 91711, USA*
[b]*Geomechanics–Rock Fracture Group, Department of Geological Sciences 172, Mackay School of Mines, University of Nevada, Reno, NV 89557, USA*
[c]*Department of Geosciences, Trinity University, 715 Stadium Drive, San Antonio, TX 78212, USA*

Received 21 August 2000; accepted 5 March 2002

Abstract

Seismic refraction profiling and gravity measurements along the length of the northern Devils Lane graben in Canyonlands National Park reveal that the bedrock floor of the graben is buried beneath a sedimentary cover more than 90 m thick, at least four to ten times more fill than previously measured. This sediment thickness, when combined with exposed fault topography, yields a throw of ≥145 m on the master fault. We estimate that horizontal extensional strain across the graben is on the order of 2–3%, and if this is typical of grabens elsewhere in Canyonlands the maximum average strain rates across the region are about $1 \times 10^{-14}\ s^{-1}$, or ~2 mm $year^{-1}$. Our results indicate that published length to displacement relationships underestimate fault offset at Devils Lane by a factor of at least 1.5. This suggests that careful geophysical evaluation of sediment thickness elsewhere within the Canyonlands graben system, an important 'type area' for investigating the mechanics which characterize the formation of kilometer-scale extensional faults, may be required before these structures can be used to help define accurate fault length to displacement scaling laws.

Keywords: Graben; Geophysical exploration; Fault; Development; Extension

1. Introduction

For the past two decades ongoing study of the actively deforming system of geologically young grabens exposed in the Needles District of Canyonlands National Park, Utah has yielded important insight into graben geometry and the mechanics of graben formation (e.g. McGill and Stromquist, 1979; Trudgill and Cartwright, 1994; Cartwright et al., 1995; Cartwright and Mansfield, 1998; Moore and Schultz, 1999; Schultz-Ela and Walsh, 2002). The grabens deform a thick sequence (~450 m) of Pennsylvanian to Early Permian clastic sedimentary rocks, as shown in Fig. 1 (Lewis and Campbell, 1965; Condon, 1997). These clastic units overlie the Pennsylvanian Paradox evaporite sequence, dipping ~4°NW toward the Colorado River down the flank of the Monument upwarp. Stresses produced as a result of the river's rapid incision through the clastic sequence are thought to be responsible for the incremental development of the graben system over at least the past 60–65 ka (Huntoon, 1982; Biggar and Adams, 1987; Schultz-Ela and Walsh, 2002). The need to understand fault development and scaling relationships (e.g. Cowie and Scholz, 1992a; Gillespie et al., 1992; Cartwright et al., 1995, 2000; Clark and Cox, 1996; Moore and Schultz, 1999; Schultz, 1999; McGill et al., 2000), particularly for large faults, is underscored by their importance in such diverse fields as petroleum exploration, where an understanding of the factors which control graben geometry in extensional settings can play a role in predicting the location and size of oil reservoirs (e.g. Jackson, 1995), and planetary geology, where grabens are commonly used to calculate regional strain (e.g. Davis et al., 1995; Schultz, 1997).

In general, the large number of young, cleanly exposed normal faults makes Canyonlands an almost ideal location to study the relationship between fault trace length and dip-slip displacement for a single population of kilometer-scale normal faults. In spite of the accessibility of the faults above the surface, however, a sequence of alluvial, colluvial and aeolian sediments obscures the bedrock floor of the hanging wall block in most locations (e.g. McGill and Stromquist, 1979; Moore and Schultz, 1999), complicating direct

* Corresponding author.
E-mail address: ebg04747@pomona.edu (E.B. Grosfils).

0191-8141/03/$ - see front matter © 2002 Elsevier Science Ltd. All rights reserved.
PII: S0191-8141(02)00040-8

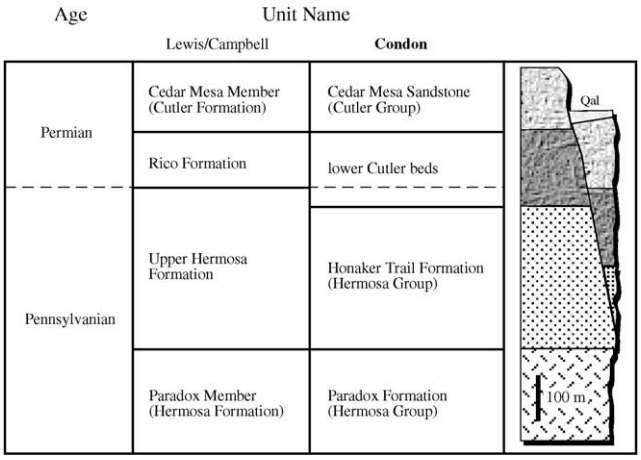

Fig. 1. Abridged stratigraphic section for Needles District grabens, after Lewis and Campbell (1965) and Condon (1997), showing penetration of faults toward the Paradox.

measurement of dip-slip displacement. Previous estimates of sedimentary fill thickness vary considerably. For instance, a sediment cover of <14 m is invoked to evaluate the age and rate of graben initiation (Biggar and Adams, 1987), while others suggest that sediment thickness may range from 5 m to perhaps >50 m (Trudgill and Cartwright, 1994). More recently, as part of the most comprehensive fault scaling study conducted to date in the region, Cartwright et al. (1995) collected length and displacement data for 97 normal faults. Where the hanging wall block was obscured by sediment, estimates of the fill thickness—guided where possible by observations of blocks of Cedar Mesa sandstone interpreted as downfaulted caprock in stream sections, fissures and swallow holes—were used to determine fault displacement (see also Cartwright and Mansfield, 1998). Measured sedimentary sequence thicknesses vary from 0.5–12 m, with the majority of values falling in the 3–7 m range. Unfortunately, Cartwright et al. (1995) do not state how many measurements were made, in which grabens, or how these values were translated into total sediment thickness, only that the maximum error in their fault displacement values (error in surveyed fault offset plus, where applicable, estimated sediment thickness) is everywhere $<10\%$. Unless sediment thicknesses significantly greater than measured values were assumed, however, it is reasonable to infer that even the fault with the greatest dip-slip displacement ($\sim$150 m; see fig. 3 of Cartwright et al., 1995) should not contain sediments thicker than about 25 m (i.e. 12 m + 0.1 × 150 m), implying visible scarp topography of about 125 m, consistent with published measurements (e.g. Moore and Schultz, 1999). More typical maximum fill values within the majority of the grabens surveyed by Cartwright et al. (1995), given a 10% error for maximum fault displacements of $\sim$20–80 m (see their fig. 3) plus measured sediment sections 3–7 m thick, should be on the order of 5–15 m.

There is, however, an additional concern which to our awareness is not addressed in any previously published studies of fault displacement within the Canyonlands region. Does the maximum fault displacement occur where the observed bounding scarp-height is greatest, as is commonly assumed, or is it possible that lesser scarp heights elsewhere along the length combine with greater sediment thickness to yield the maximum displacement? Direct field measurements of sediment thickness collected systematically along the length of any given graben are required to assess the location and magnitude of the maximum fault displacement. Thus, we hypothesize that there could be considerable error in existing estimates of maximum fault displacement due to uncertainty about variations in along-axis sediment thickness, and argue that this issue requires further consideration. We show that the locations of maximum footwall uplift along the master and antithetic faults, and of maximum sediment thickness, do not necessarily coincide, revealing the sequence of development (faulting and deposition) for particular grabens (e.g. Cartwright and Mansfield, 1998; Morley, 1999).

When combined with the physical restrictions imposed by the delicacy of the cryptogamic ecosystems present in this part of the national park, the need for systematic along-axis measurement of sediment thicknesses motivates the use of noninvasive geophysical techniques that complement ongoing collection of structural data above the surface. Here we present the results from a shallow geophysical survey designed to evaluate sediment thickness along the length of the northern segment of Devils Lane graben (Fig. 2). One of the more frequently studied grabens in Canyonlands National Park, northern Devils Lane is a medium-sized example 3.5 km long from tip to tip and <200 m wide. Structural ramps capped by jointed Cedar Mesa sandstone (Condon, 1997) accommodate fault displacement near the ends of the graben (e.g. Trudgill and Cartwright, 1994), but sediments obscure the central 2.4 km of the hanging wall, and previous measurements of the maximum observable dip-slip displacement (i.e. scarp height) vary from 83 to 100 m for the master fault (Trudgill and Cartwright, 1994; Moore and Schultz, 1999). Our results, which reveal sediment thicknesses exceeding 90 m, indicate that previous sediment thickness estimates in northern Devils Lane are at least four to ten times too small, a difference that is of some concern since Canyonlands is a ‘type area’ for

Fig. 2. Aerial photograph of Devils Lane graben. The inset diagram shows the location of Canyonlands National Park in Utah, an aerial view of part of the grabens system with the confluence of the Green and Colorado rivers marked by a star, and a box surrounding the northern part of Devils Lane graben shown in the main part of the figure. In the larger image of Devils Lane the sediment fill covering the graben floor is dark while higher elevation, jointed Cedar Mesa sandstone caps the horsts on either side. Geophysical data, including both seismic refraction (spreads 1–12) and gravity measurements (stations 1–14), were collected near the center of the graben at the locations shown.


109°52'W
UTAH
GS07
11
GS06
10
GS05
Paleochannel
Paleochannel
BS01
9
GS04
Paleochannel
GS01
8
GS08
GS02
BS02
7
GS03
GS10
GS09
&
BS03
6
Paleochannel
38°08'N
38°08'N
GS11
GS14
4
5
GS12
3
12
GS13
1
2
S.O.B.
Hill
500 m
Seismic Refraction Spread
Gravity Station
Surveying Base Station
109°52'W

characterizing graben scaling relationships and mechanics. While it is not yet known how sediment thickness varies along-axis for other grabens in the region, it is reasonable to conclude that further geophysical studies are necessary to establish sediment thicknesses and hence fault displacements with certainty, and thus that both length to displacement scaling relations for the area (Cartwright et al., 1995) and rates of extension across the province (Moore and Schultz, 1999) may require revision.

2. Methods

After an initial seismic reconnaissance (Bush et al., 1996), seismic refraction and gravity data were collected in the summer of 1999 in order to gain a better understanding of sediment thickness as a function of position along the length of the northern Devils Lane graben. Twelve spreads of P-wave refraction data were acquired using a 24-channel Geometrics Strataview seismograph, 10-Hz geophones and a sledgehammer energy source. Ten of the spreads, laid out along the N–S axis of the graben to minimize interference from talus adjacent to graben walls, covered a total length of nearly 2 km (Fig. 2), while the remaining spreads were oriented roughly perpendicular to the graben walls to try to constrain the dip of the graben floor. Geophone spacing for all but two of the along-axis spreads was 10 m while the cross-spread geophone spacing used was 3 m. Three to five shot points were used with each spread. Center-shot and end-shot offsets of 5 m were acquired to resolve the properties of shallow layers, while end-shot offsets of 60 m were acquired to resolve layers at greater depths. The maximum offset was limited to 290 m both by available cable length and the ability to generate significant energy through the poorly consolidated surface sediment. Examples of field records are shown in Figs. 3 and 4. First-breaks were picked independently by Grosfils and Kroeger as well as with automatic picking software. The results were virtually identical, with only a dozen picks at the longest offsets showing significant variation. These few discrepancies were resolved by identifying coherent arrivals across adjacent records. The seismic data were then modeled using an iterative inversion refraction analysis software package (SIPT2) in which the first solution is generated by a delay-time method while subsequent iterations modify the solution with ray tracing (Scott, 1973); results are shown in Figs. 5 and 6. The sediment thickness values obtained, when combined with high precision topography collected by Moore and Schultz (1999), were used to determine total fault offset (Fig. 7).

To complement the seismic study, gravity data were collected at 15 stations using a Worden gravimeter. All 15 stations were established on or near the graben's N–S axis (Fig. 2), and their relative vertical and horizontal positions were surveyed using a Sokkia Set4A total field station. Measurements were repeated at the gravity base station (GS01) every 2 h or less to facilitate linear drift corrections, and all standard post-processing to correct for latitude, elevation and topography (cf. Burger, 1992) used this station's position as the local datum. The Bouguer anomaly was calculated using an assumed density of 2.6 g cm^{-3}, chosen from standard tables (Burger, 1992) as representative of the sedimentary rock types found within the grabens district (Fig. 1). Local terrain corrections used to adjust the Bouguer anomaly were performed using a cylindrical Hammer grid superimposed upon 1:24000 scale U.S. Geological Survey topographic maps. The topography within rings A–C was not taken into account due to both an absence of rigorous topographic control at this scale ($<$16.64 m from the gravity station) and the qualitative field observation that the topography along the graben floor varies minimally over this distance. We note that even if floor topography as extreme as 5 m was ignored as a result (a value far greater than any local variations observed), the total error accrued would be $\sim$0.004 mgal, or far less than 1%. The local Hammer terrain correction was also not applied for rings H and outwards ($>$1.5 km from the gravity station) as ignoring the topography present at these distances yields comparably negligible error. The raw results from the complete gravity reduction have a distinctively U-shaped appearance (Fig. 8a). To model the anomaly we use a linearly detrended version of the data (Fig. 8b), which should predominantly reflect the anomalous gravitational signature of the shallow, unconsolidated sedimentary fill. While this assumption is somewhat simplistic, it is important to note that gravity interpretations from a single line are non-unique, implying that use of more complicated subsurface models is unwarranted. Our objective is simply to gain an independent constraint that can be used to test the plausibility of our preferred seismic refraction interpretation.

3. Results

3.1. Seismic results

The character of the travel time curves for the seven contiguous along-axis seismic spreads (Figs. 5a and 6a) is extremely consistent along the entire length of the data. At small increasing offsets, apparent velocities rise gradually from about 350 m s^{-1} to between 700 and 900 m s^{-1} where they remain relatively constant. These velocities imply a layer of loose sand and gravel or alluvium (e.g. Burger, 1992), an interpretation consistent with the surface sediments in the graben. The clearly parallel sets of forward and reverse travel time curves show the consistency of these velocities along the axis of the graben.

On spreads 12, 3, 4, 8 and 9, a sharp break in apparent velocity occurs at longer offsets, with velocity values jumping to over 2000 m s^{-1}. On spreads 12, 3 and 4, these apparent velocities are distinctly asymmetric between forward and reverse shots suggesting a sharp, dipping interface

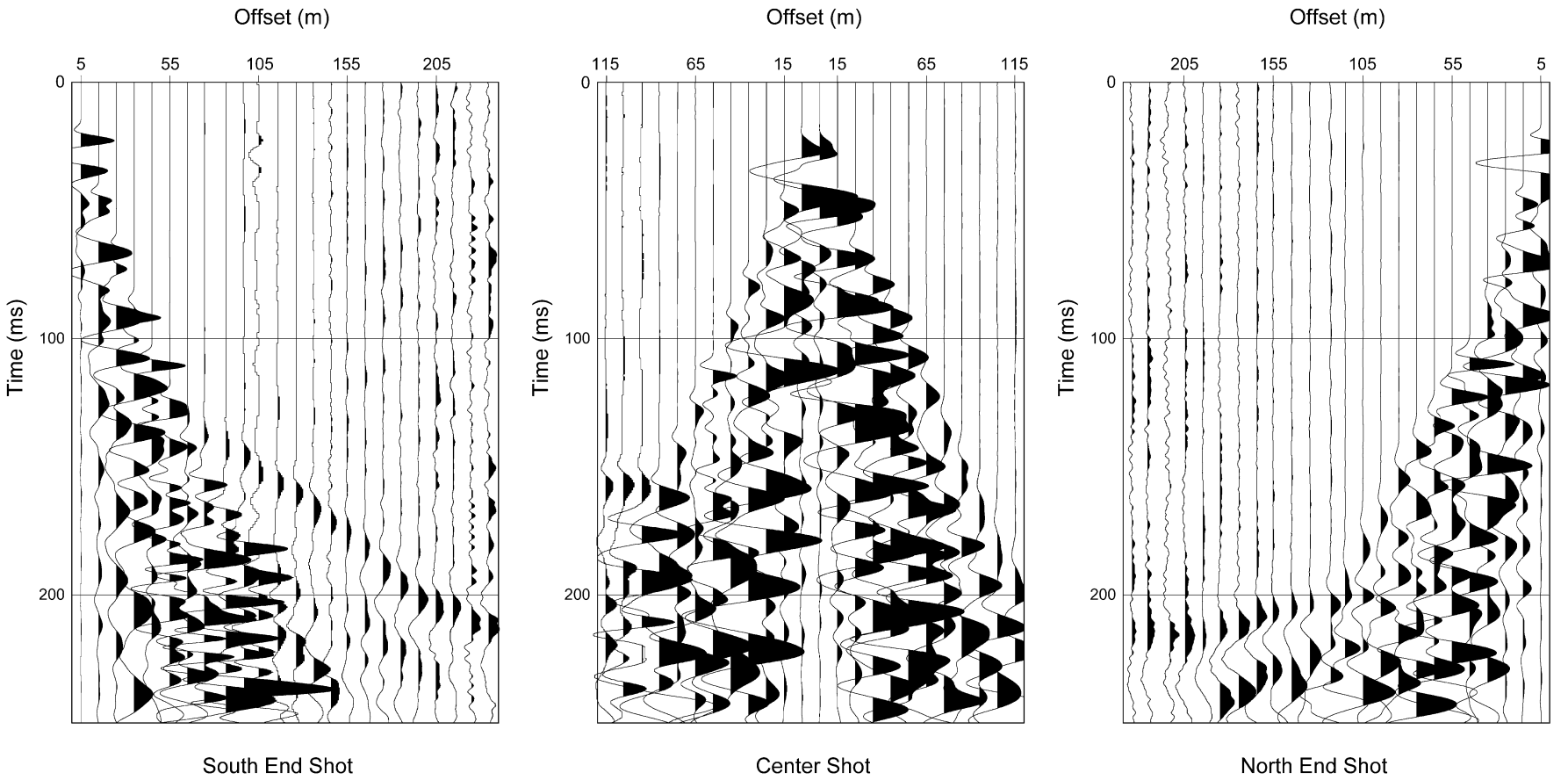

Fig. 3. Seismic field records (shot gathers) from geophone spread 12 in northern Devil's Lane graben (see Fig. 2 for location). The left panel shows the records from the forward shot at the south end of the spread, 5 m offset from geophone 1. The break from apparent velocities less than 1000 m s^{-1} to apparent velocities greater than 2000 m s^{-1}, which we interpret to result from the sediment–bedrock interface, occurs at an offset of approximately 60 m. The right panel shows the records from the reverse shot at the north end of the spread, 5 m offset from geophone 24. The corresponding break occurs at an offset of approximately 110 m and exhibits a higher apparent velocity. This asymmetry between the forward and reverse shots indicates a sediment–bedrock interface dipping northward. The center panel shows the records from the center spread shot, midway between geophones 12 and 13. The asymmetry in these records also indicates a northward-dipping interface with a break to high apparent velocities visible in the shallower up-dip direction, and absent in the down dip direction.

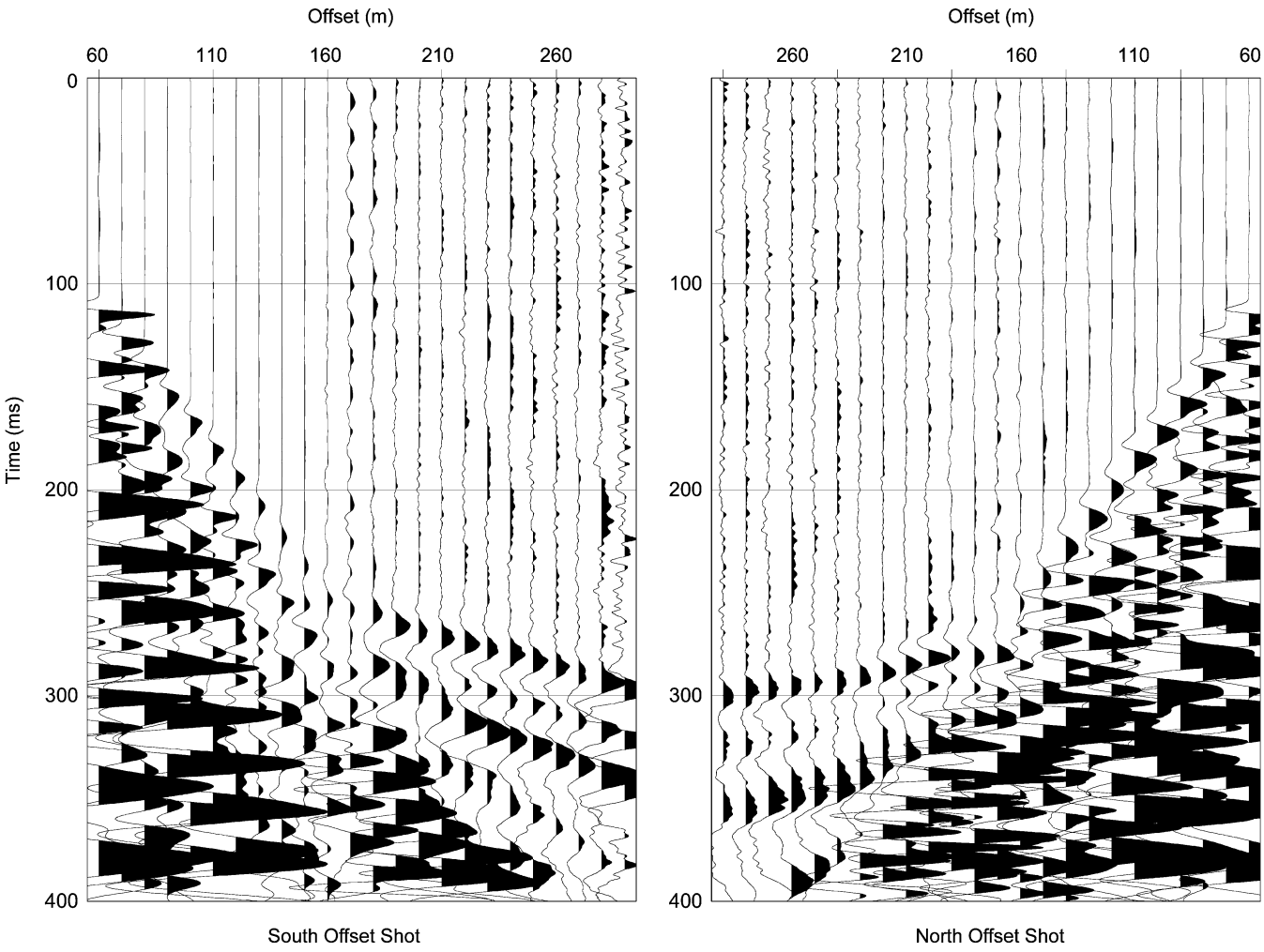

Fig. 4. Seismic field records (shot gathers) from geophone spread 9 in northern Devil's Lane graben (see Fig. 2 for location). The sharp break between arrivals with apparent velocities less than 1000 m s^{-1} and apparent velocities of approximately 3000 m s^{-1} are nearly symmetric in the forward and reverse shots indicating a sharp subhorizontal interface between the sediment and bedrock. These breaks occur at offsets of approximately 180 m in both directions.

(Figs. 3 and 5a). Irregularities in the apparent velocities suggest a few meters of topography on this interface. On spreads 8 and 9 (Figs. 4 and 6a) the apparent velocities observed on forward and reverse shots are approximately equal, suggesting a sharp subhorizontal interface. The break between sub-1000 m s^{-1} velocities and velocities of about 3000 m s^{-1} occurs at offsets of approximately 180 m (Fig. 4). On spreads 6 and 7 the break to apparent velocities over 2000 m s^{-1} is observed only on the longest offsets of some shots, indicating that the maximum depth to bedrock occurs beneath these lines (Fig. 6). When corrected for dip, the velocities obtained for these arrivals ranges from 2900 to 3600 m s^{-1} with an average of 3200 m s^{-1}. We interpret these velocities to represent the Cedar Mesa sandstone bedrock beneath the unconsolidated sediment fill. Velocities around 3200 m s^{-1} are within the range typical for sandstones studied elsewhere (e.g. Burger, 1992), and are clearly not representative of uncompacted sediment. Furthermore, velocities obtained directly from acoustic well log data elsewhere in Canyonlands range from 3100 to 5000 m s^{-1} for 'Cedar Mesa equivalent' sandstone at depths of 400–600 m (Mineral Canyon 1 well, Enserch Exploration Inc.) to 3300–5700 m s^{-1} for the Cutler Formation as a whole at depths of about 600–800 m (Buck Mesa 1 well, Husky Oil Company, interpreted by Kanbur et al. (2000)). Our velocities fall at the lower end of the ranges observed in the acoustic logs, a result which is qualitatively consistent with the significantly shallower depth of burial for the jointed Cedar Mesa sandstone within Devils Lane.

For interpreting the seismic data, we adopt a three-layer model. The shallowest layer encapsulates the very low velocity of the sediments near the surface. Arrivals with apparent velocities under 500 m s^{-1} were assigned to this layer. Although the data show no sharp break in velocity and thus no sharp interface between these and deeper sediments, this layer allows us to preserve these lowest velocities in the model for more accurate ray tracing and better depth estimates for the deeper interface. Processing each spread and correcting apparent velocities for dip yields a velocity of 405 m s^{-1} for this layer. The second layer is chosen to

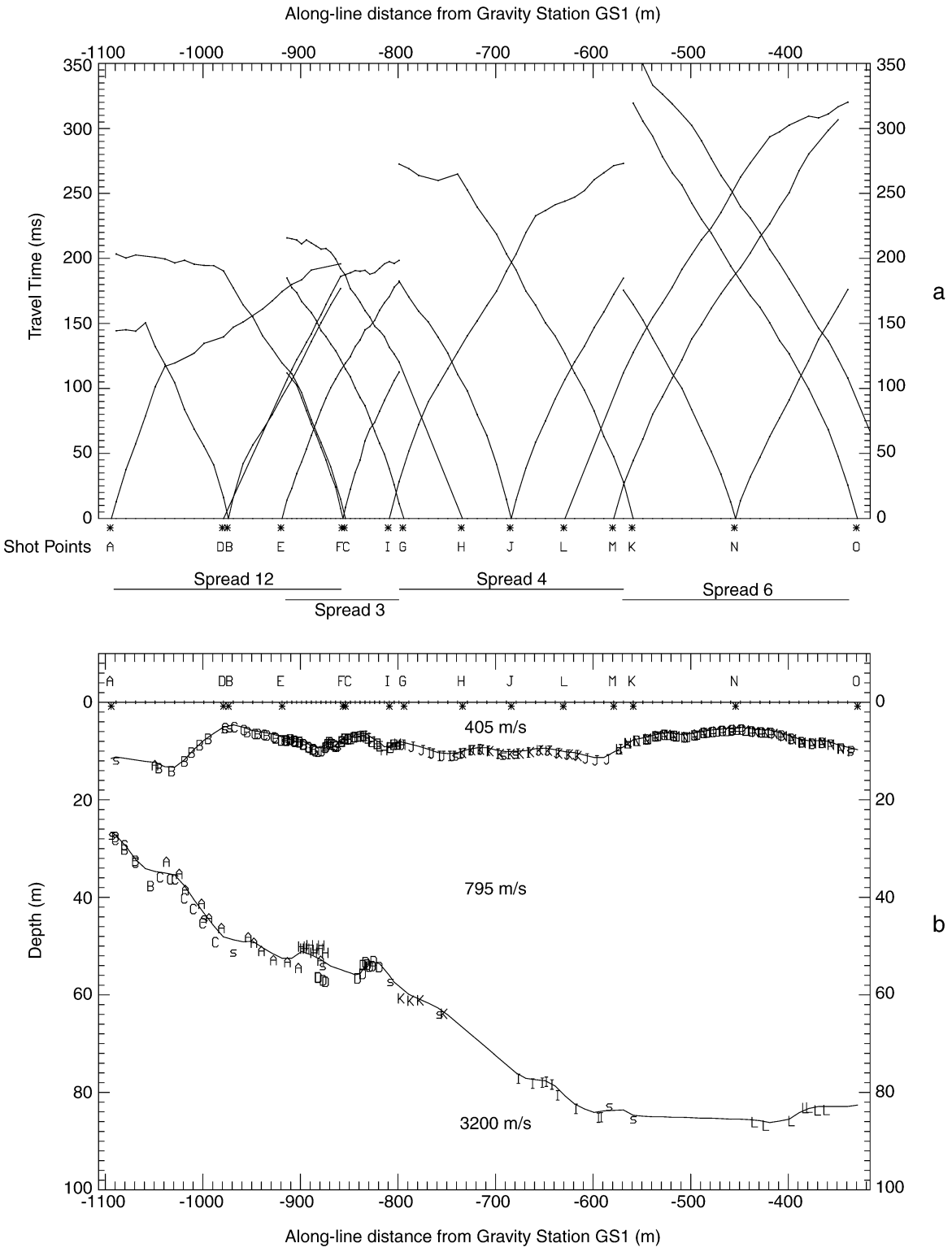

Fig. 5. (a) First break travel time curves for seismic spreads 12, 3, 4 and 6. Geophone positions are plotted along the combined line relative to gravity station GS01 (located at $x = 0$). Shot points are lettered A–O. Slow velocities (<500 m s^{-1}) of shallow sediment are represented by the initial steep sections of the curves. The long parallel sections of the curves have apparent velocities of between 700 and 850 m s^{-1}. Sharp breaks to velocities greater than 2500 m s^{-1} are visible on many of the curves with longer offsets. These velocities occur at greater offsets moving north along the line, indicating the increasing depth of the sediment–bedrock interface. (b) Three-layer model resulting from the travel time curves. The model was generated with SIPT2 software that employs iterative ray tracing to refine an initial delay-time model (Scott, 1973). Letters indicate ray entry and exit points along the two subsurface interfaces. The dipping sediment–bedrock interface is well constrained beneath spreads 12 and 3 where there is good reciprocal coverage of this interface. Beneath spreads 4 and 6, this interface is deeper, and while clearly present is not as well constrained by our data due to limited geophone offsets.

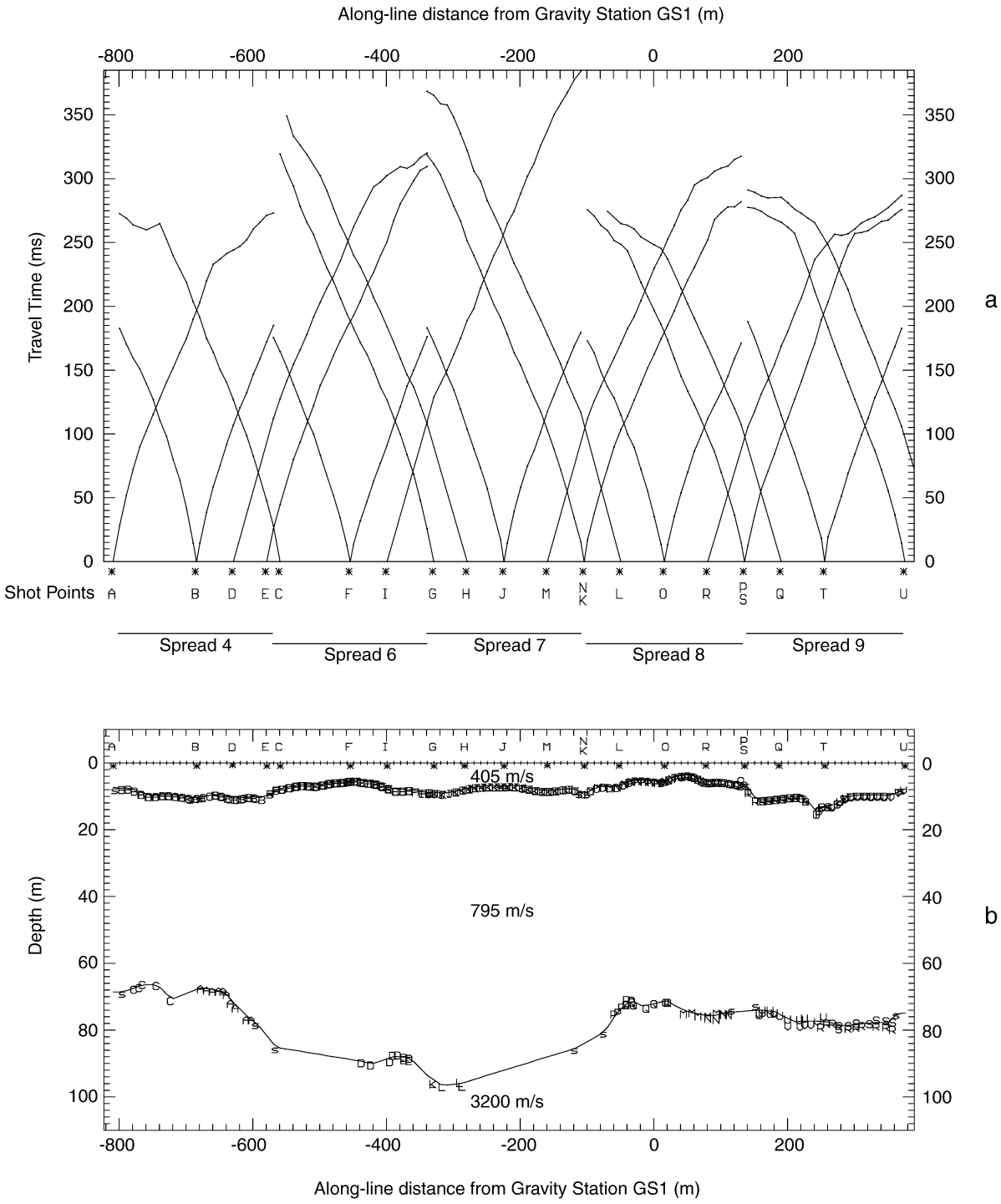

Fig. 6. (a) First break travel time curves for seismic spreads 4 and 6–9. Geophone positions are plotted along the combined line relative to gravity station GS01. Shot points are lettered A–U. Slow velocities (<500 m s^{-1}) of shallow sediment are represented by the initial steep sections of the curves. The long parallel sections of the curves have apparent velocities of between 700 and 850 m s^{-1}. Sharp breaks to velocities greater than 2500 m s^{-1} are visible on many of the curves with longer offsets. This break is not observed on the long offsets for spreads 6 and 7 indicating greater depth to bedrock beneath these spreads. (b) Three-layer model resulting from the travel time curves. The model was generated with SIPT2 software that employs iterative ray tracing to refine an initial delay-time model (Scott, 1973). Letters indicate ray entry and exit points along the two subsurface interfaces. The subhorizontal sediment–bedrock interface is well constrained beneath spreads 8 and 9 where there is good reciprocal coverage of this interface. Beneath spreads 6 and 7, this interface is deeper, and while clearly present is not as well constrained by our data due to limited geophone offsets.

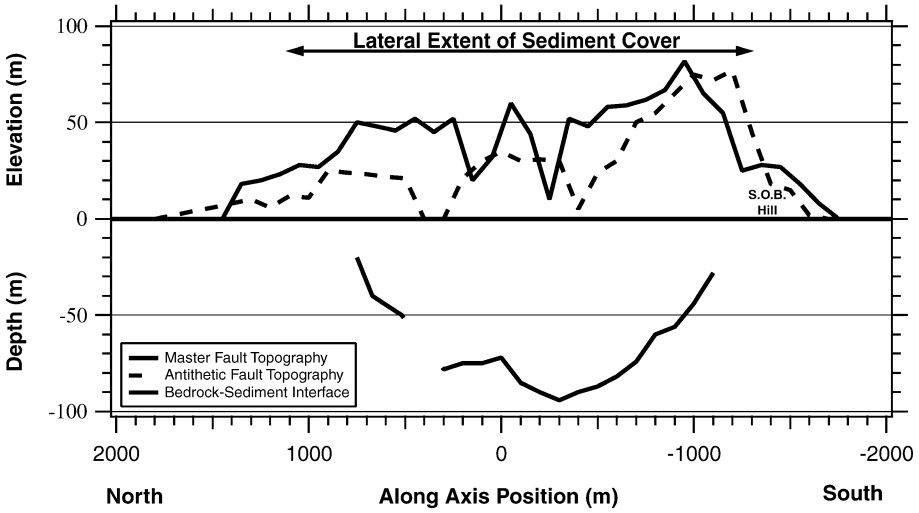

Fig. 7. A cross-section compilation of seismic modeling results and topography for Devils Lane graben. An elevation of zero marks the sediment-filled floor of the graben, an along-axis position of zero coincides with the location of GS01 in Fig. 2, and the lateral extent of the sediment cover is indicated. Above the surface the topography of the master (NW) fault is shown as a thick solid line and that of the antithetic (SE) fault is depicted as a dashed line (adapted from Moore and Schultz, 1999); paleochannel erosion has produced pronounced V's in the topography data at two locations. Below the surface the depth to the bedrock interface as inferred from seismic data (Figs. 5 and 6) sampled at 100 m intervals is shown as a solid line; depths beneath spread 11 are not continuous with the rest of the data. The maximum depth to bedrock observed, 93 m, is a minimum estimate, and the maximum dip-slip offset observed, 145 m, is also a minimum value (see text). The maximum offset observed occurs roughly 350 m south of the zero mark, a position which does not coincide closely with the location of the maximum surface topography (950 m south of zero), and both seismic and gravity data suggest that the actual depth to bedrock may be 10–20 m deeper near the center of the graben.

represent the bulk of the arrivals that show consistent apparent velocities of between 700 and 900 m s^{-1}. Processing each spread to correct the apparent velocities for dip yields an average velocity of 795 m s^{-1} for this layer. The third layer, representing all velocities over 2000 m s^{-1} (there were no apparent velocities between 900 and 2000 m s^{-1}) yields an average dip-corrected velocity of 3200 m s^{-1}.

The depth model resulting from inversion of the data is shown in Figs. 5b and 6b. The result from spreads 12, 3, 4 and 6, shown in Fig. 5b, shows the bedrock dipping strongly northward from depths of 30 m in the south (just north of S.O.B. Hill; Fig. 2) to depths of over 90 m beneath spread 6. The result from spreads 4 and 6–9, shown in Fig. 6b, shows the bedrock interface rising from depths of over 90 m beneath spreads 6 and 7 to depths of 70–78 m beneath spreads 8 and 9. The letters along the interface represent entry and exit points of the ray tracing. The exit points are lettered according to the corresponding shot points. The entry and exit points for many shot points are tightly clustered along this interface beneath spreads 12, 3, 4, 8 and 9 indicating that these are the best resolved segments of the sediment-bedrock interface. These are also the areas with good reciprocal (forward and reverse shot) coverage of the sediment bedrock interface. Because of the greater depths beneath spreads 6 and 7, and the limits of our shot-receiver offsets, we do not have good reciprocal coverage and the exact depth and topography of the interface is not as well constrained in this area. We varied the bedrock velocity and some layer assignments in the inversion to investigate the degree of uncertainty beneath line 6 and 7. This analysis resulted in variations in depth of up to 10 m. The model presented in Fig. 6b represents the shallowest depths obtained.

Of the remaining five seismic spreads, the two cross spreads and two of the along-axis spreads confirm the velocities for the sediment, but were too short to detect the bedrock interface. The final along-axis spread, spread 11 (see Fig. 7), was not contiguous with the others and was modeled independently. Picking P-wave first arrivals for this spread was difficult, in part because the graben is narrower, and although all three layers clearly exist there is more uncertainty in the resulting depth model than for the other along-axis spreads. At the north end of spread 11, the depth to bedrock is well constrained at 20 m. At the south end of the spread, 45–50 m is the most plausible interpretation, but the bedrock could be as shallow as 35 m at this location.

Depths to bedrock extracted from the model at 100 m intervals are shown in Fig. 7 co-aligned with the high precision footwall fault scarp topography collected by Moore and Schultz (1999). These depths were also used as a starting point for modeling the gravity data.

3.2. Gravity results

We model the linearly detrended Bouguer anomaly data using the 2D software package GravModel (Burger, 1992), and begin with a starting cross-section based directly on interpretation of our seismic results (Fig. 8c). This initial model, given a density contrast of -0.25 g cm^{-3} (i.e. an

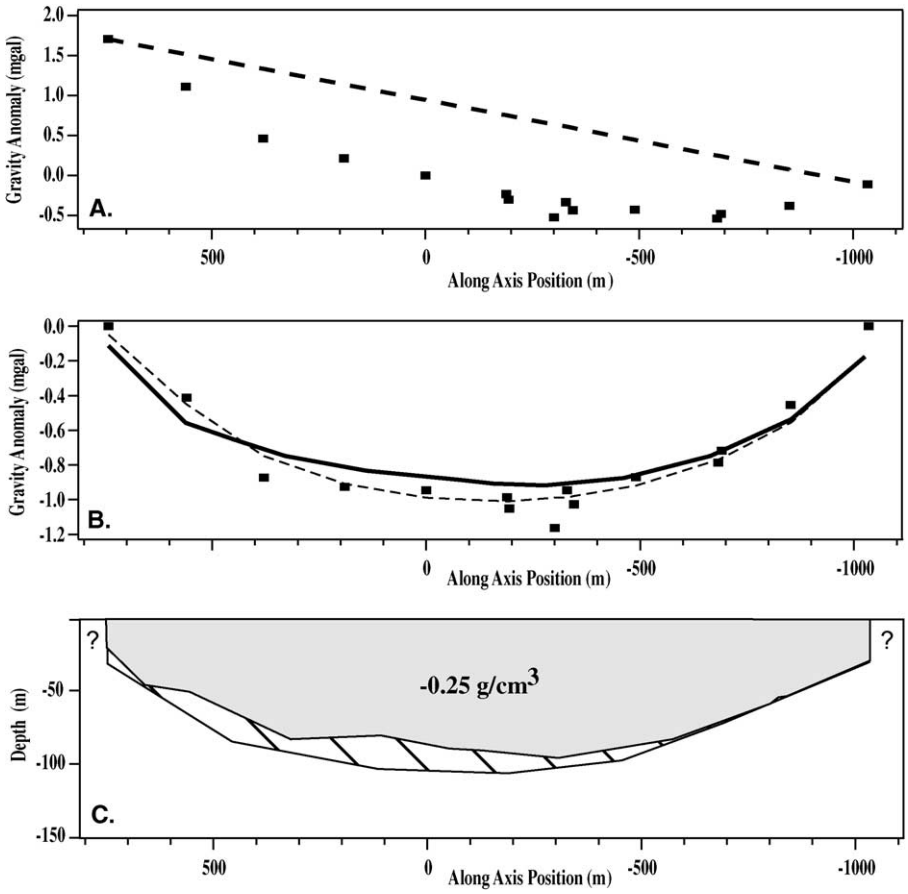

Fig. 8. Gravity analysis for Devils Lane. (a) Raw, terrain corrected Bouguer anomaly for Devils Lane, locally referenced to the value at gravity station 01 (GS01); see text for details. An along-axis position of zero coincides with the location of GS01 in Fig. 2. Each dot represents the gravity anomaly measured at a single station, and the dashed line indicates the regional gravity gradient. (b) Raw, detrended gravity data (dots). The solid line is the gravity model produced using depths inferred from the seismic refraction data (Figs. 5 and 6) and a density contrast of -0.25 g cm^{-3} between the sediment and underlying bedrock. The dashed line is a model yielding a better fit, produced using the same density contrast and a slightly greater depth to bedrock near the center of the graben, a modification consistent with the seismic data which probably underestimate depth to bedrock in this region. (c) Cross-sectional geometries used to model the gravity data; model results are shown in (b). The gray shaded cross-section is the depth model taken directly from the seismic refraction interpretation, and the diagonally hachured region shows the depth modifications required to yield a model which more closely fits the raw detrended gravity data.

effective average density of 2.35 g cm^{-3} for the sediments since 2.6 g cm^{-3} was assumed for the bedrock), yields a reasonable fit to the data (Fig. 8b). A minimal geometric modification to this starting model, in which the depth of the sedimentary fill near the center of the graben is increased by 10–15 m, more closely matches the gravity anomaly data. Since the seismic model upon which the initial cross-section was based provides a minimum depth to the sediment-bedrock interface, this result is encouraging. If the sediment grains have the same average density as was assumed for the host rock (2.6 g cm^{-3}) or consist predominantly of quartz (2.7 g cm^{-3}), a -0.25 g cm^{-3} density contrast implies an average porosity of 15–20%, a range that is a bit low for an unpacked sand aggregate surface deposit but reasonable as an average for a deposit tens of meters thick where the packing geometry is characterized by greater loading, especially given a range of grain sizes and shapes (e.g. Leeder, 1982). Thus we conclude that, given a plausible density variation between the unconsolidated sediments and underlying bedrock, a single along-axis geometry for the graben fill, as summarized in Fig. 7, is consistent with both the seismic and gravity data.

4. Discussion

4.1. Length-displacement relationship

Several studies have focused upon characterizing the length to displacement geometry of the Canyonlands grabens in a systematic fashion. Cartwright et al. (1995) report maximum dip-slip offset values for 97 normal faults with tip-to-tip trace lengths ranging from ~100 to 6500 m, whereas Cartwright and Mansfield (1998) and Moore and Schultz (1999) evaluate offset in detail along the length of several individual, well-exposed grabens. All three studies assume that exposed bounding fault topography approximates total structural offset in the Needles District (e.g.

McGill and Stromquist, 1979; Trudgill and Cartwright, 1994; Cartwright et al., 1995), and therefore that sediment thickness variations and other sources introduce fairly minimal error (e.g. <10%; Cartwright et al., 1995) into dip-slip offset measurements for the grabens in Canyonlands National Park. In Devils Lane, visible scarp heights measured from the cap rock of the adjacent horsts to the upper surface of the sediment occupying the graben vary from a minimum of zero at the fault tips to a maximum of 83 m approximately three-quarters of the way down the N–S length of the graben (Moore and Schultz, 1999). Using previously published measurements of sediment thickness in the grabens of Canyonlands (everywhere <12 m; Cartwright et al., 1995) and a 10% displacement error, the maximum dip-slip offset on the Devils Lane master fault inferred from previous studies should be ≤105 m (83 m + 12 m + 10% error of 9.5 m), a value consistent with length to displacement fault data collected in many areas other than Canyonlands (e.g. Gillespie et al., 1992; Schlische et al., 1996).

When variations in along-axis topography and the depth to bedrock determined in this study are combined (as shown in Fig. 7), it becomes apparent that the maximum dip-slip offset on the master fault is ≥145 m, a value which occurs at a position roughly 350 m south of GS01 (our zero reference position). This offset value is a minimum since possible erosional reductions in surface topography are ignored (paleochannel activity has clearly modified portions of the scarp near this location) and the sediment thickness determined from the seismic model, as reported above, is also a minimum value. Even when this minimum value is compared with the maximum value of 105 m inferred previously, however, the dip-slip offset measured in this study is half again as great as was earlier recognized. Note that, had the greatest sediment thickness (93 m) and the greatest scarp topography (83 m) simply been added together without considering their along-axis location, the dip-slip offset inferred for Devils Lane would have been substantially greater. Similarly, had the greatest scarp topography simply been combined with a sediment thickness estimate at that location, the dip-slip offset inferred would also have been incorrect.

The relationship between fault length and displacement, determined for faults ranging over several orders of magnitude in size, is described by the power law equation:

$$D_{\max} = \gamma L^n, \tag{1}$$

where $D_{\max}$ and L are maximum (relative) displacement and horizontal length, γ is a scaling constant, and n is approximately unity (e.g. Cowie and Scholz, 1992a; Clark and Cox, 1996). Given a graben length of ~3200 m along the master fault (Moore and Schultz, 1999), $D_{\max}/L$ (i.e. the value of the scaling constant γ) is increased from ≤0.033 ($D_{\max} \leq 105$ m) to ≥0.045 ($D_{\max} \geq 145$ m) using our revised values of the structural offset. If Devils Lane is a typical Canyonlands graben, published length to displacement analyses for Canyonlands (Cartwright et al., 1995) may underestimate the maximum fault offset by about a factor of 1.5, placing the offset values near the upper part of the range observed elsewhere for faults of this length (e.g. Cowie and Scholz, 1992a; Clark and Cox, 1996; Schultz, 1997). We note as well that preliminary seismic work conducted during the summer of 2000 in Cyclone Canyon, a 4.4-km-long graben in the Canyonlands system, also reveals sediment thicknesses well in excess of 12 m, suggesting that Devils Lane is not unique in this regard.

4.2. Strain

The strain accommodated by the Devils Lane graben can be estimated by using two complementary approaches. First, the volumetric strain associated with the graben is given by:

$$\epsilon_h = (DLH)/V \tag{2}$$

where D is the average displacement along each bounding fault, L is the horizontal fault length, H is the down-dip fault height, and V is the volume of the region containing the graben; the quantity DLH is the total geometric moment of the structure (e.g. Scholz, 1997). Fault dips (δ) in Devils Lane are generally steep, with $\delta = 65$–$75°$ (e.g. McGill and Stromquist, 1979). For the master fault, $D = (0.47D_{\max}) \times \cos\delta$ (Moore and Schultz, 1999) = 18 m ($D_{\max} = 145$ m, $\delta = 75°$), $L = 3200$ m and $H = [450 \text{ m}/\cos(90 - \delta)] = 466$ m; for the antithetic fault (where D is roughly 70% that of the master fault), $D = (0.33D_{\max}) \times \cos\delta$ (Moore and Schultz, 1999) = 15 m ($D_{\max} = 130$ m, $\delta = 70°$), $L = 3500$ m and $H = [450 \text{ m}/\cos(90 - \delta)] = 479$ m. The geometric moments for the master and antithetic graben-bounding faults are 27×10^6 m^3 and 25×10^6 m^3, respectively, with a combined moment for the graben of 52×10^6 m^3. Assuming a volume defined by the fault length and layer thickness (e.g. Cowie et al., 1993), with the fault-normal dimension related to the maximum extent of footwall uplift or antithetic rollover anticline (~500 m on either side of the fault), the volume is $(3200 \times 450 \times 500 \text{ m}^3) = 720 \times 10^6$ m^3 for the master fault, $(3500 \times 450 \times 500 \text{ m}^3) = 788 \times 10^6$ m^3 for the antithetic fault, and 1508×10^6 m^3 for both faults. Thus, the extensional strain ϵ_h (Eq. (2)) is approximately 3%. The major uncertainties in the volumetric extensional strain are the dip of the antithetic fault and the volume calculated for the sedimentary layer.

As a second way to evaluate strain, the shear strain parallel to a fault is proportional to $D_{\max}/L$ (Cowie and Scholz, 1992b). Following Schultz and Fossen (2002), the horizontal (extensional) component ϵ_h of the fault-parallel shear strain is obtained from the scaling relations by

$$\epsilon_h = \cos(\delta)(D_{\max}/L). \tag{3}$$

This method (Mège and Reidel, 2001; Schultz and Fossen, 2002) implicitly incorporates off-fault deformation through its contribution to $D_{\max}$ measured along the fault, in a

volume comparable with that used in Eq. (2). Following this approach, the horizontal (extensional) normal strain for the Devils Lane master fault is 1.2% using the revised value of maximum displacement ($D_{max} \geq 145$ m) and $\delta = 75°$. With displacement ($D_{max} \geq 130$ m) on the antithetic fault, we estimate the total extensional strain accommodated by the northern Devils Lane graben (using the updated values of fault displacement) to be 2.2%. Both the volumetric and D–L scaling approaches for calculating the extensional strain yield comparable values. These values are much smaller than previous strain estimates made using approximate methods of balanced cross-sections and rigid-block kinematics (e.g. Moore and Schultz, 1999) but are consistent with recent numerical models of graben growth in the Canyonlands area (Schultz-Ela and Walsh, 2002). This suggests that simplifying assumptions (e.g. rigid-block kinematics and uniform rock properties) and simple geometric operations (e.g. area or line-length balancing) employed previously may not apply well to faulting of highly jointed rocks such as those found in Canyonlands, where the deformation may be modulated by the presence of both open and closed joints.

4.3. Strain rate

If the Canyonlands graben system has been developing for at least the past 60–65 ka (Biggar and Adams, 1987), a net horizontal strain of ~2% across the deforming region (having an original cross-strike dimension of 5.2 km (Moore and Schultz, 1999)) implies a maximum average strain rate of about 1×10^{-14} s^{-1}, equivalent to an extension rate of approximately 2 mm year^{-1}. These strain rate and extension rate values are consistent with recent numerical modeling results (Schultz-Ela and Walsh, 2002), but the values should be considered approximate since the timing of graben initiation within Canyonlands requires further refinement. The time used in our strain rate calculation is based on Biggar and Adam's (1987) dating of sediment collected near the base of a swallow hole <14 m deep in one of the western grabens and assumes that the sample location coincides with the total depth of the sedimentary sequence. The rate calculation also assumes uniform extension across the graben-deformed province, which may be a poor approximation given suggestions that extension initiated near the Colorado River and spread outward from it (McGill and Stromquist, 1979; Huntoon, 1982; Moore and Schultz, 1999), which would lead to spatially variable rates of extension; however, the good agreement between our values and the modeling results of Schultz-Ela and Walsh (2002), which explicitly allow non-uniform extension, help ameliorate this concern. Because geodetic techniques such as GPS have sufficient sensitivity to measure deformation rates in the calculated range, the rates of extensional deformation and, perhaps, the age of graben inception—the parameters now having the greatest uncertainty—can also be constrained by appropriate geodetic field campaigns.

5. Conclusions

Interpretation of seismic refraction and gravity data collected along the length of northern Devils Lane indicates that sediment thickness in this medium size Canyonlands graben is greater than 90 m, four to ten times thicker than previous maximum estimates for the graben system as a whole. When sediment thickness as a function of position is combined with the topography of the exposed portions of the master fault, the net throw for northern Devils Lane is inferred to be ≥145 m, at least 1.5 times the dip-slip offset inferred from earlier studies. We estimate that the net horizontal strain for the northern Devils Lane graben is on the order of 2–3%, and note that maximum average strain rates of about 1×10^{-14} s^{-1} for the section of the graben system studied by Moore and Schultz (1999) imply extension of ~2 mm year^{-1}, a rate an order of magnitude less than suggested by previous calculations. If the sediment thickness observed in northern Devils Lane is representative of other grabens in the Canyonlands system, existing D–L relationships derived for this area also underestimate fault offset by a factor of 1.5. Continued geophysical study of additional grabens in the area, preferably in conjunction with continued structural analysis, sediment dating and a geodetic campaign to evaluate modern strain rates, will help establish whether or not Devils Lane is a typical Canyonlands graben, further improving our understanding of this important and intriguing extensional fault system.

Acknowledgements

We would like to thank the participants of the 1996 and 1999 Canyonlands Grabens Initiatives for their contributions to the geophysical work performed in Devils Lane, John Louie for fruitful discussions about seismic velocities in the Canyonlands area, and Ken Herkenhoff for providing a copy of the Mineral Canyon well log data. We also express our gratitude to the personnel of the National Park Service (especially Charlie Schelz) for facilitating access to the grabens; to Bob Burger and Linda Reinen for their comments; and, to Joe Cartwright, Jim Evans and Zoe Shipton for their thoughtful reviews. This work was supported in part by grants from NASA's Planetary Geology and Geophysics Program to R.A. Schultz, the NSF to Glenn Kroeger (NSF EHR DUE 9851222), and Summer Undergraduate Research Program funding from Pomona College.

References

Biggar, N.E., Adams, J.A., 1987. Dates derived from Quaternary strata in the vicinity of Canyonlands National Park. In: Campbell, J.A. (Ed.), Geology of Cataract Canyon and Vicinity: Four Corners Geological Society, 10th Field Conference Guidebook, pp. 127–136.

Burger, H.R., 1992. Exploration Geophysics of the Shallow Subsurface. Prentice Hall, New Jersey.

Bush, N.I., Harris, C., Grosfils, E.B., 1996. Refraction seismology in Devils

Lane graben, Canyonlands National Park, Utah [abs]. Eos (Transactions, American Geophysical Union) 77, F643.

Cartwright, J.A., Mansfield, C.S., 1998. Lateral displacement variation and lateral tip geometry of normal faults in Canyonlands National Park, Utah. Journal of Structural Geology 20, 3–19.

Cartwright, J.A., Trudgill, B.D., Mansfield, C.S., 1995. Fault growth by segment linkage: an explanation for scatter in maximum displacement and trace length data from the Canyonlands Grabens of SE Utah. Journal of Structural Geology 17, 1319–1326.

Cartwright, J.A., Trudgill, B.D., Mansfield, C.S., 2000. Fault growth by segment linkage: an explanation for scatter in maximum displacement and trace length data from the Canyonlands Grabens of SE Utah: reply. Journal of Structural Geology 22, 141–143.

Clark, R.M., Cox, S.J.D., 1996. A modern regression approach to determining fault displacement–length relationships. Journal of Structural Geology 18, 147–152.

Condon, S.M., 1997. Geology of the Pennsylvanian and Permian Cutler Group and Permian Kaibab limestone in the Paradox Basin, southeastern Utah and southwestern Colorado. U.S. Geological Survey Bulletin 2000, 1–46.

Cowie, P.A., Scholz, C.H., 1992a. Displacement–length scaling relationships for faults: data synthesis and discussion. Journal of Structural Geology 14, 1149–1156.

Cowie, P.A., Scholz, C.H., 1992b. Physical explanation for the displacement–length relationship of faults using a post-yield fracture mechanics model. Journal of Structural Geology 14, 1133–1148.

Cowie, P.A., Scholz, C.H., Edwards, M., Malinverno, A., 1993. Fault strain and seismic coupling on mid-ocean ridges. Journal of Geophysical Research 98, 17,911–17,920.

Davis, P.A., Tanaka, K.L., Golombek, M.P., 1995. Topography of closed depressions, scarps and grabens in the north Tharsis region of Mars: implications for shallow crustal discontinuities and graben formation. Icarus 114, 403–422.

Gillespie, P.A., Walsh, J.J., Watterson, J., 1992. Limitations of displacement and dimension data for single faults and the consequences for data analysis and interpretation. Journal of Structural Geology 14, 1157–1172.

Huntoon, P.W., 1982. The Meander anticline, Canyonlands, Utah—an unloading structure resulting from horizontal gliding on salt. Geological Society of America Bulletin 93, 941–950.

Jackson, M.P.A., 1995. Retrospective salt tectonics. In: Jackson, M.P.A., Roberts, D.G., Snelson, S. (Eds.), Salt tectonics—a global perspective. American Association of Petroleum Geologists Memoir 65, pp. 1–28.

Kanbur, Z., Louie, J.N., Chavez-Perez, S., Plank, G., Morey, D., 2000. Seismic reflection study of Upheaval Dome, Canyonlands National Park, Utah. Journal of Geophysical Research 105, 9489–9505.

Leeder, M.R., 1982. Sedimentology: Process and Product. George Allen & Unwin, London.

Lewis Sr, R.Q., Campbell, R.H., 1965. Geology and uranium deposits of Elk Ridge and vicinity, San Juan County, Utah. U.S. Geological Survey Professional Paper 474, 1–69.

McGill, G.E., Stromquist, A.W., 1979. The grabens of Canyonlands National Park, Utah—geometry, mechanics and kinematics. Journal of Geophysical Research 84, 4547–4563.

McGill, G.E., Schultz, R.A., Moore, J.M., 2000. Fault growth by segment linkage: an explanation for scatter in maximum displacement and trace length data from the Canyonlands Grabens of SE Utah: discussion. Journal of Structural Geology 22, 135–140.

Mège, D., Reidel, S.P., 2001. A method for estimating 2D wrinkle ridge strain from application of fault displacement scaling to the Yakima folds, Washington. Geophysical Research Letters 28, 3545–3548.

Moore, J.M., Schultz, R.A., 1999. Processes of faulting in jointed rocks of Canyonlands National Park, Utah. Geological Society of America Bulletin 111, 808–822.

Morley, C.K., 1999. Patterns of displacement along large normal faults: implications for basin evolution and fault propagation, based on examples from East Africa. American Association of Petroleum Geologists Bulletin 83, 613–634.

Schlische, R.W., Young, S.S., Ackerman, R.V., Gupta, A., 1996. Geometry and scaling relations of a population of very small rift related normal faults. Geology 24, 683–686.

Scholz, C.H., 1997. Earthquake and fault populations and the calculation of brittle strain. Geowissenschaften 15, 124–130.

Schultz, R.A., 1997. Displacement–length scaling for terrestrial and Martian faults: implications for Valles Marineras and shallow planetary grabens. Journal of Geophysical Research 102, 12009–12015.

Schultz, R.A., 1999. Understanding the process of faulting: selected challenges and opportunities at the edge of the 21st century. Journal of Structural Geology 21, 985–993.

Schultz, R.A., Fossen, H., 2002. Displacement–length scaling in three dimensions: the importance of aspect ratio and application to deformation bands. Journal of Structural Geology 24, 1389–1411.

Schultz-Ela, D.D., Walsh, P., 2002. Modeling of grabens extending above evaporites in Canyonlands National Park, Utah. Journal of Structural Geology 24, 247–275.

Scott, J.H., 1973. Seismic refraction modeling by computer. Geophysics 28, 271–284.

Trudgill, B., Cartwright, J., 1994. Relay-ramp forms and normal-fault linkages, Canyonlands National Park, Utah. Geological Society of America Bulletin 106, 1143–1157.